Structural and superionic properties of Ag^+-rich ternary phases within the AgI–MI_2 systems

2002 J. Phys.: Condens. Matter 14 13579

(http://iopscience.iop.org/0953-8984/14/49/313)

INSTITUTE OF PHYSICS PUBLISHING JOURNAL OF PHYSICS: CONDENSED MATTER

J. Phys.: Condens. Matter **14** (2002) 13579–13596 PII: S0953-8984(02)39526-2

Structural and superionic properties of Ag^+-rich ternary phases within the AgI–MI_2 systems

S Hull[1], **D A Keen**[1,2] **and P Berastegui**[3]

[1] The ISIS Facility, Rutherford Appleton Laboratory, Didcot, Oxon OX11 0QX, UK
[2] Physics Department, Oxford University, Parks Road, Oxford OX1 3PU, UK
[3] Arrhenius Laboratory, Stockholm University, S-106 91 Stockholm, Sweden

Received 16 July 2002
Published 29 November 2002
Online at stacks.iop.org/JPhysCM/14/13579

Abstract

The effects of temperature on the crystal structure and ionic conductivity of the compounds Ag_2CdI_4, Ag_2ZnI_4 and Ag_3SnI_5 have been investigated by powder diffraction and impedance spectroscopy techniques. ε-Ag_2CdI_4 adopts a tetragonal crystal structure under ambient conditions and abrupt increases in the ionic conductivity are observed at 407(2), 447(3) and 532(4) K, consistent with the sequence of transitions ε-$Ag_2CdI_4 \rightarrow \beta$-$Ag_2CdI_4 + \beta$-AgI + $CdI_2 \rightarrow \alpha$-AgI + $CdI_2 \rightarrow \alpha$-Ag_2CdI_4. Hexagonal β-Ag_2CdI_4 is metastable at ambient temperature. The ambient-temperature β phase of Ag_2ZnI_4 is orthorhombic and the structures of β-Ag_2CdI_4 and β-Ag_2ZnI_4 can, respectively, be considered as ordered derivatives of the wurtzite (β) and zincblende (γ) phases of AgI. On heating Ag_2ZnI_4, there is a 12-fold increase in ionic conductivity at 481(1) K and a further eightfold increase at 542(3) K. These changes result from decomposition of β-Ag_2ZnI_4 into α-AgI + ZnI_2, followed by the appearance of superionic α-Ag_2ZnI_4 at the higher temperature. The hexagonal crystal structure of α-Ag_2ZnI_4 is a dynamically disordered counterpart to the β modification. Ag_3SnI_5 is only stable at temperatures in excess of 370(3) K and possesses a relatively high ionic conductivity ($\sigma \approx 0.19\ \Omega^{-1}\ cm^{-1}$ at 420 K) due to dynamic disorder of the Ag^+ and Sn^{2+} within a cubic close packed I^- sublattice. The implications of these findings for the wider issue of high ionic conductivity in AgI–MI_2 compounds is discussed, with reference to recently published studies of Ag_4PbI_6 and Ag_2HgI_4 and new data for the temperature dependence of the ionic conductivity of the latter compound.

1. Introduction

Silver iodide, AgI, is one of the most widely studied superionic compounds. Under ambient conditions it usually exists as a two-phase mixture of the cubic zincblende structured γ phase ($F\bar{4}3m$, $a = 6.495$ Å, $Z = 4$ [1]) and the hexagonal wurtzite structured β phase ($P6_3mc$, $a = 4.592$ Å, $c = 7.510$ Å, $Z = 2$ [2]). These comprise cubic close packed (ccp) and hexagonal

close packed (hcp) anion sublattices, respectively, and both contain two tetrahedral and one octahedral cavity per anion (or per cation). As befits the significant covalent character of the interionic bonding, the Ag^+ are ordered over the tetrahedral sites, such that the AgI_4 tetrahedra share only corners. At $T = 420$ K AgI undergoes the transition to its superionic α phase, with an increase in ionic conductivity, σ, of over three orders of magnitude to a value $\sim 2\ \Omega^{-1}\ cm^{-1}$ (for a review of the superionic properties of AgI, see [3]). The essentially rigid anion sublattice forms a body centred cubic (bcc) array and the Ag^+ undergo rapid jump diffusion between tetrahedral cavities via sites which are trigonally co-ordinated [4]. It is generally accepted that the octahedral interstices play little or no role in the conduction process [5].

Significant research effort has been expended in the search for ternary derivatives of AgI with improved superionic behaviour. In particular, the addition of M^{2+} cations provides some reduction in the superionic transition temperature. However, this is not as low as room temperature (see [6] and references therein) and it occurs at the cost of significant reductions in σ within the superionic phase. These factors, coupled with the high cost of silver containing compounds, have seriously restricted the commercial possibilities for such compounds in, amongst others, solid state battery applications. Nevertheless, the mechanism by which chemical doping influences the structure–property relationships within AgI derivatives is of significant fundamental importance and has motivated a number of studies of Ag-rich AgI–MI_2 systems by the authors [6–8] and others [9–17]. In this paper we consider AgI–MI_2 with $M = Cd^{2+}$, Zn^{2+}, Sn^{2+}, Hg^{2+} and Pb^{2+}, with specific emphasis on the first three.

In the phase diagram of the AgI–CdI_2 system a single intermediate phase of composition Ag_2CdI_4 is found [9, 10]. Under ambient conditions the ionic conductivity is relatively low ($\sim 10^{-7}\ \Omega^{-1}\ cm^{-1}$ [11]) and the crystal structure of Ag_2CdI_4 under ambient conditions has been proposed to be tetragonal (ε-phase, $a \sim 6.35$ Å, $c \sim 12.7$ Å [9, 10]) or hexagonal (β-phase, $a \sim 4.578$ Å, $c \sim 7.529$ Å [12]). The principal difficulty lies in the low synthesis temperature necessary to produce Ag_2CdI_4. The tetragonal ε form is favoured if long-term annealing (several months) is performed below ~370 K, whereas the hexagonal β phase (together with β-AgI) is observed in samples quenched from higher temperatures [10]. Two transitions observed in ionic conductivity studies at ~370 and ~450 K have been attributed to one of two sequences: ε-$Ag_2CdI_4 \rightarrow \beta$-$Ag_2CdI_4 \rightarrow \alpha$-AgI + CdI_2 [10] or ε-$Ag_2CdI_4 \rightarrow \beta$-AgI + $CdI_2 \rightarrow \alpha$-AgI + CdI_2 [9], the latter publication reporting that the β form of Ag_2CdI_4 is a metastable phase formed on cooling.

Similar confusion surrounds the properties of the corresponding composition within the AgI–ZnI_2 system. Thermal studies by Fourcroy *et al* [13] proposed that Ag_2ZnI_4 decomposes at 469 K, with two further endothermal features observed at 545 and 595 K being interpreted as sublimation of ZnI_2 and the eutectic temperature of the system. Ammlung *et al* [14] interpreted their ionic conductivity and Raman scattering data in terms of a phase transition in Ag_2ZnI_4 at 418 K, followed by incongruent melting at 429 K. The most recent study using x-ray diffraction and DTA methods [15] attributed the former to the $\beta \rightarrow \alpha$ transition in unreacted AgI and, instead, suggested that Ag_2ZnI_4 exists in two distinct temperature ranges. On heating, the ambient temperature β form decomposes to form a two-phase mixture of β-AgI and ZnI_2 at 477 K but then reforms at 538 K (as α-Ag_2ZnI_4), before decomposing again at 553 K. Under ambient conditions, the crystal structure of β-Ag_2ZnI_4 was originally indexed on the basis of hexagonal 'wurtzite-like' unit cells with $a \sim 4.39$ Å and $c \sim 7.33$ Å [10, 13]. However, Blachnik and Stöter [15] observed that, whilst the intense diffraction peaks could be accounted for by such a unit cell, additional weaker reflections required the use of a larger orthorhombic unit cell with $a = 11.731(6)$ Å, $b = 13.344(3)$ Å and $c = 7.304(3)$ Å. No detailed structural information has been published for the α-Ag_2ZnI_4 phase either, merely a list of the d-spacings of eight diffraction lines collected at 550 K [15].

The phase diagram of the AgI–SnI_2 system is more complex. Blachnik and Stöter [16] identified three compounds of compositions Ag_3SnI_5, $AgSn_2I_5$ and $AgSn_4I_9$. These were subsequently confirmed by Wojakowski *et al* [17]. The first was shown to possess a very wide compositional range with the lowest temperature of its stability region (382 K) occurring at the stoichiometry Ag_3SnI_5. This phase shows high ionic conductivity ($\sigma \sim 0.1$–$0.4\ \Omega^{-1}\ cm^{-1}$) and is stable up to its incongruent melting temperature of 636 K [17]. X-ray diffraction studies show that the diffraction peaks are consistent with a ccp unit cell with $a \sim 6.30$ Å [16], though no information on the ionic positions has been reported.

The remaining two systems AgI–PbI_2 and AgI–HgI_2 have been studied recently and their structural behaviour is understood [6–8]. In the former case, a superionic phase centred around a stoichiometry of Ag_4PbI_6 exists at temperatures in excess of ≈420 K [8]. This phase has a high ionic conductivity ($\sigma \sim 0.1\ \Omega^{-1}\ cm^{-1}$) and adopts a ccp anion sublattice ($Fm\overline{3}m$, $a = 6.3317(2)$ Å, $Z = 2/3$ at 455(2) K [8]) in which the two cation species are dynamically disordered predominantly over the octahedral interstices, though with a small fraction (∼5%) residing within the tetrahedral cavities. The structural behaviour of the Ag^+-rich phase in the AgI–HgI_2 system, Ag_2HgI_4, is more complex. Under ambient conditions the β phase possesses a slightly distorted ccp I^- sublattice ($I\overline{4}$, $a = 6.3194(3)$ Å, $c = 12.606(1)$ Å, $Z = 2$ at 298(2) K [6]) in which the Ag^+ and Hg^{2+} are ordered over 3/4 of the tetrahedral interstices occupied by Ag^+ in γ-AgI. At 326(2) K Ag_2HgI_4 undergoes a superionic transition to the α phase with a 50-fold increase in σ. α-Ag_2HgI_4 also adopts a ccp anion sublattice ($F\overline{4}3m$, $a = 6.3337(1)$ Å, $Z = 1$ at 338(2) K [6]), with the two cation species disordered over half the tetrahedral cavities. Further transitions are observed at ∼410 and ∼445 K to phases labelled δ and ε, respectively [7]. These are also cation disordered superionic phases, though formed by hcp ($P6_3/mmc$, $a = 4.4833(1)$ Å, $c = 7.3252(3)$ Å, $Z = 1/2$ at 430(2) K [7]) and bcc ($Im\overline{3}m$, $a = 5.0160(1)$ Å, $Z = 1/2$ at 338(2) K [7]) anion sublattices, respectively. The behaviour of the ionic conductivity within the δ and ε phases of Ag_2HgI_4 has not been reported to date.

2. Experimental details

Samples of Ag_2CdI_4, Ag_2ZnI_4 and Ag_3SnI_5 were prepared by solid state reaction of appropriate quantities of the constituent binary halides, whilst commercially available Ag_2HgI_4 supplied by Strem Chemicals Inc. was used. Sintering at 373(3) K for six weeks with intermediate grindings was required to form a single-phase ε-Ag_2CdI_4 sample. At temperatures in excess of ∼393K, partial decomposition to AgI and CdI_2 was observed. In the case of β-Ag_2ZnI_4, the sample was annealed for four weeks at 453(3) K. Attempts to synthesize the material at lower temperatures or for shorter times produced samples with a crystal structure closely related to that of β-Ag_2ZnI_4 (see section 3.3) but with incomplete ordering of the two cation species. Ag_3SnI_5 is only stable at elevated temperatures ($\gtrsim$380 K [17]) and was prepared '*in situ*' during the diffraction experiment. The samples of Ag_2ZnI_4 and Ag_3SnI_5 were sealed in thin-walled silica ampoules (12 mm diameter and ∼35 mm in length) and the neutron diffraction experiments performed on the Polaris powder diffractometer at the ISIS facility, UK [18]. High-temperature measurements used a special furnace designed for neutron diffraction constructed using vanadium foil resistive heating element and heat shields. Diffraction data were predominantly collected using the detector bank which covers the scattering angles $83° < \pm 2\theta < 97°$ and provides data over the d-spacing range $0.5 < d\ (Å) < 4.3$ with a resolution $\Delta d/d \sim 7 \times 10^{-3}$. In view of the exceptionally high neutron absorption cross-section of Cd, the diffraction studies on Ag_2CdI_4 were restricted to ambient-temperature x-ray measurements of the samples following heat treatments using a STOE/STADIP diffractometer with Cu Kα_1 radiation. Rietveld profile refinements of the powder diffraction data were performed using the program GSAS [19].

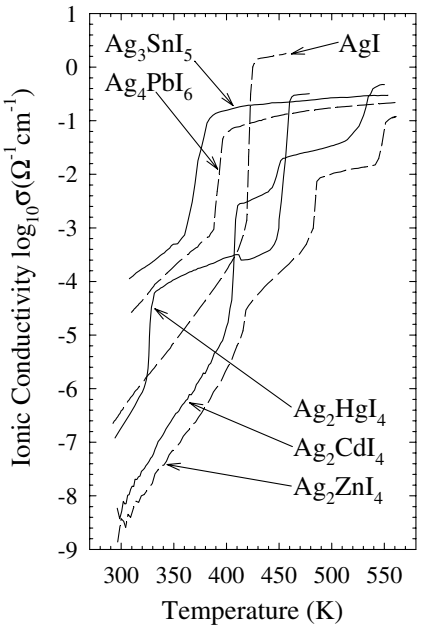

Figure 1. The temperature variation of the ionic conductivity, $\log_{10}\sigma$, for Ag_2CdI_4, Ag_2ZnI_4, Ag_2HgI_4, Ag_3SnI_5, Ag_4PbI_6 and AgI. The data for the latter two compounds are taken from [8].

Thermal characterization of the Ag_2CdI_4 samples was carried out using a Perkin–Elmer DSC 2C instrument in the temperature range 300–575 K, with the powder in sealed capsules and at heating and cooling rates of 10 K min^{-1}. Temperature calibration was performed using a standard In sample. Two terminal measurements of the ionic conductivity were performed using pellets of ∼5.0 mm diameter and ∼5.2 mm length held between two spring loaded platinum discs inside a boron nitride cell which is inserted into the hot zone of a horizontal tube furnace. Details of this device can be found elsewhere [20]. A Solartron S1260 frequency response analyser determined the conventional Z–Z' Bode plots over the frequency range from 10^{-1} to 10^7 Hz. The real component of the sample impedance, Z_S, was determined using software developed in house [20]. Measurements were performed under dynamic vacuum of $\sim 10^{-5}$ bar, except those for Ag_2HgI_4, which were made with the sample sealed under a slight over pressure of argon to prevent the loss of volatile HgI_2 at elevated temperatures [6].

3. Results

3.1. Ionic conductivity measurements

The temperature dependence of the ionic conductivities of the four compounds Ag_2CdI_4, Ag_2ZnI_4, Ag_3SnI_5 and Ag_2HgI_4 is illustrated in figure 1, together with the data for Ag_4PbI_6 and AgI published previously [8]. The behaviour of Ag_2CdI_4 and Ag_3SnI_5 is in broad agreement with that reported in the literature for Ag_2CdI_4 [11] and Ag_4SnI_6 [17]. Measurements of Ag_3SnI_5 and Ag_4SnI_6 confirm that their conductivities are indeed very similar, with the latter having a value ∼10% lower in the superionic regime. Both Ag_2CdI_4 and Ag_3SnI_5 undergo abrupt increases in their ionic conductivity, σ, of around two orders of magnitude at relatively low temperatures (407(2) and 370(3) K, respectively) and Ag_2CdI_4 shows two smaller jumps

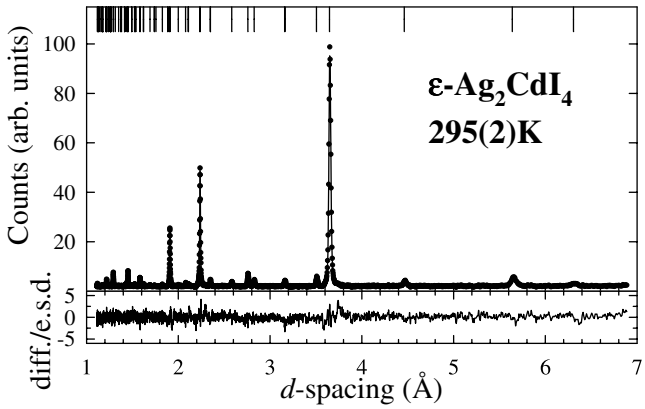

Figure 2. The least-squares fit to the powder x-ray diffraction data collected from ε-Ag_2CdI_4 at 295(2) K. The dots are the experimental data points (with fitted background subtracted) and the solid curve is the calculated profile using the parameters listed in table 1. The lower trace shows the difference (measured minus calculated) divided by the estimated standard deviation on the experimental data points. The upper row of tick marks along the top of the figure denotes the calculated positions of all the symmetry allowed Bragg reflections for space group $I\bar{4}2m$.

at 447(3) and 532(4) K. In the case of Ag_2ZnI_4, a small discontinuity in σ at 420(1) K can be attributed to the $\beta + \gamma \rightarrow \alpha$ transition within a small quantity of unreacted AgI in the sample, whilst the two subsequent jumps at 481(1) and 542(3) K presumably correspond to the transitions observed by DTA methods by Blachnik and Stöter at 477 and 538 K [15]. At temperatures below ∼400 K the behaviour of the ionic conductivity of Ag_2HgI_4 agrees well with that reported previously [6], whilst the data collected at higher temperatures show a slight decrease in σ ($\sigma_\delta \sim 0.8\sigma_\alpha$) at the $\alpha \rightarrow \delta$ transition observed at 412(2) K and a large increase in σ ($\sigma_\varepsilon \sim 690\sigma_\delta$) at the $\delta \rightarrow \varepsilon$ transition which occurs at 454(6) K.

3.2. X-ray diffraction results: Ag_2CdI_4

The x-ray diffraction data collected from the sample of ε-Ag_2CdI_4 could be indexed using a tetragonal unit cell of dimensions $a \approx 6.33$ Å and $c \approx 12.68$ Å. Reflection conditions were hkl, $h + k + l = 2n$; $hk0$, $h + k = 2n$; $0kl$, $k + l = 2n$; hhl, $l = 2n$; $00l$, $l = 2n$; $h00$, $h = 2n$. These are consistent with eight different space groups. Of these, $I\bar{4}$ and $I\bar{4}2m$ were considered initially, since they represent two plausible candidate structures adopted by β-Ag_2HgI_4 and β-Cu_2HgI_4, respectively [6]. Trial refinements of the x-ray diffraction data from ε-Ag_2CdI_4 were performed using each of these structures. However, only the latter gave a satisfactory fit to the data ($R_W = 4.95\%$), with the final fitted parameters listed in table 1. The quality of the fit to the experimental diffraction data is illustrated in figure 2.

In order to investigate the high-temperature hexagonal β-Ag_2CdI_4 phase, x-ray diffraction analyses were performed at room temperature on samples annealed at temperatures between 395(3) and 455(3) K. No significant differences were observed between samples that had been quenched or slowly cooled after different lengths of time. It is evident that a partial decomposition of tetragonal ε-Ag_2CdI_4 into CdI_2 and β-AgI occurs above 395(3) K. Additional peaks from a new phase appear above 405(3) K but the fractional weight of this phase remains nearly constant at higher temperatures. A careful analysis of the positions and intensities of all the observed reflections reveals six non-overlapping reflections that can be attributed to the new phase and indexed using a hexagonal unit cell with $a = 4.483(3)$ Å and

Table 1. Summary of the results of the least-squares refinements of the diffraction data collected from ε-Ag_2CdI_4, β-Ag_2ZnI_4, α-Ag_2ZnI_4 and Ag_3SnI_5. u_{iso} is the mean-square amplitude of the isotropic thermal vibrations and m is the site occupancy, defined such that the total for a given ion gives its population within a single unit cell. The weighted and expected R-factors are given by $R_W^2 = \sum_{N_d} \frac{(y_{obs}-y_{calc})^2}{(\sigma y_{obs})^2} / \sum_{N_d} \frac{(y_{obs})^2}{(\sigma y_{obs})^2}$ and $R_{exp}^2 = (N_d - N_p) / \sum_{i=1}^{N_d} \frac{(y_{obs})^2}{(\sigma y_{obs})^2}$ and the summations are made over the N_d data points used in the fit. N_v is the number of fitted variables. y_{obs} and y_{calc} are the observed and calculated intensities, respectively, and σy_{obs} is the estimated standard deviation on y_{obs} derived from the counting statistics. The Bragg R-factor is given by $R_{Bragg}^2 = \sum_{N_p} \frac{(I_{obs}-I_{calc})^2}{(\sigma I_{obs})^2} / \sum_{N_p} \frac{(I_{obs})^2}{(\sigma I_{obs})^2}$ where the N_p Bragg peaks have observed and calculated intensities I_{obs} and I_{calc}, respectively, and σI_{obs} is the estimated standard deviation on I_{obs}.

Phase/compound	ε-Ag_2CdI_4	β-Ag_2ZnI_4	α-Ag_2ZnI_4	Ag_3SnI_5
Space group	$I\bar{4}2m$	$Pmn2_1$	$P6_3/mmc$	$Fm\bar{3}m$
Temperature (K)	295(2)	295(2)	553(3)	523(3)
Lattice parameters (Å)	$a = 6.3338(3)$ $c = 12.6807(9)$	$a = 8.799(1)$ $b = 7.6220(9)$ $c = 7.2362(2)$	$a = 4.4641(2)$ $c = 7.2691(4)$	$a = 6.3323(2)$
Ag^+ parameters	Ag in 4(d) at 0, 1/2, 1/4 $u_{iso} = 0.048(7)$ Å^2	Ag in 4(b) at x, y, z $x = 0.2499(7)$ $y = 0.1668(11)$ $z = 0.1268(11)$ $u_{iso} = 0.047(3)$ Å^2	Disordered Ag + Zn $(Ag/Zn)_{tet}$ in 4(f) 1/3, 2/3, z $z = 0.637(1)$ $m = 1.10(3)$ $u_{iso} = 0.10(6)$ Å^2	Disordered Ag + Sn $(Ag/Sn)_{tet}$ in 8(c) 1/4, 1/4, 1/4 $m = 0.64(1)$
M^{2+} parameters	Cd in 2(a) at 0, 0, 0 $u_{iso} = 0.088(6)$ Å^2	Zn in 2(a) at 0, y, z $y = 0.6877(8)$ $z = 0.1185(15)$ $u_{iso} = 0.018(1)$ Å^2	$(Ag/Zn)_{oct}$ in 2(a) at 0, 0, 0 $m = 0.40(3)$ $u_{iso} = 0.20(8)$ Å^2	$(Ag/Sn)_{oct}$ in 4(b) 1/2, 1/2, 1/2 $m = 2.56(1)$ $u_{iso} = 0.16(1)$ Å^2
I^- parameters	I in 8(i) at x, x, z $x = 0.2667(3)$ $z = 0.1183(3)$ $u_{iso} = 0.049(7)$ Å^2	I1 in 2(a) at 0, y, z $y = 0.3427(12)$ $z = 0.9921(13)$ $u_{iso} = 0.039(5)$ Å^2 I2 in 2(a) at 0, y, z $y = 0.6682(13)$ $z = 0.5034(13)$ $u_{iso} = 0.019(5)$ Å^2 I3 in 4(b) at x, y, z $x = 0.2535(6)$ $y = 0.8308(9)$ $z = 0$(fixed) $u_{iso} = 0.042(5)$ Å^2	I in 2(d) at 1/3, 2/3, 1/4 $u_{iso} = 0.094(3)$ Å^2	I in 4(a) at 0, 0, 0 $u_{iso} = 0.104(2)$ Å^2
$R_W/R_{exp}/R_{Bragg}$ (%)	4.95/4.24/8.00	1.54/1.62/3.01	1.43/1.49/1.89	1.61/1.67/2.45
N_d	3988	3148	3115	3115
N_v	16	40	22	16

$c = 7.351(7)$ Å ($c/a = 1.639(2)$). The remaining reflections can be assigned to ε-Ag_2CdI_4, β-AgI and CdI_2. However, due to severe overlap, a Rietveld analysis of the diffraction pattern was not possible. By comparing the diffraction patterns, the structure of β-Ag_2CdI_4 is evidently similar to the wurtzite structure of β-AgI and has a smaller unit cell volume than pure β-AgI due to the smaller ionic radius of Cd^{2+}. Unfortunately, the amount of Cd^{2+} that is incorporated into the structure could not be determined due to the similar x-ray scattering factors for Ag^+ and

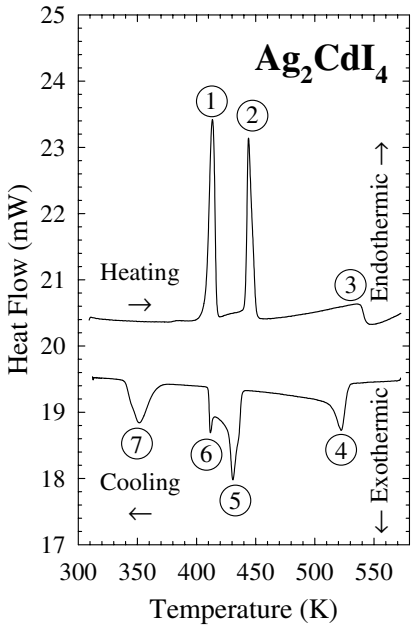

Figure 3. The DSC trace for Ag_2CdI_4 showing the thermal events during the heating and cooling cycles corresponding to ε-Ag_2CdI_4 (1) $\rightarrow$ β-AgI + CdI_2 + β-Ag_2CdI_4 (2) $\rightarrow$ α-AgI + CdI_2 (3) $\rightarrow$ α-Ag_2CdI_4 and α-Ag_2CdI_4 (4) $\rightarrow$ α-AgI + CdI_2 (5) $\rightarrow$ α-AgI + CdI_2 + β-Ag_2CdI_4 (6) $\rightarrow$ β-AgI + CdI_2 + β-Ag_2CdI_4 (7) $\rightarrow$ β-AgI + CdI_2 + β-Ag_2CdI_4 + ε-Ag_2CdI_4, respectively.

Cd^{2+} and the overlap of several reflections from the tetragonal and hexagonal phases observed in the diffraction pattern.

The DSC curve of ε-Ag_2CdI_4 exhibits three endothermic peaks at 405(2), 440(2) and 540(4) K (see figure 3) that can be assigned to the partial decomposition of ε-Ag_2CdI_4 into AgI, CdI_2 and β-Ag_2CdI_4, the transition from β-Ag_2CdI_4 to α-AgI and CdI_2 and the dissolution of CdI_2 in AgI to form α-Ag_2CdI_4 respectively, with the latter assumed to be the superionic phase. These transition temperatures are in good agreement with the observed changes of the ionic conductivity (figure 1). The DSC data for the cooling cycle show some hysteresis and the four observed thermal events can be attributed to the sequence α-Ag_2CdI_4 $\rightarrow$ α-AgI + CdI_2 (at 529(3) K) $\rightarrow$ α-AgI + CdI_2 + β-Ag_2CdI_4 (at 438(2) K) $\rightarrow$ β-AgI + CdI_2 + β-Ag_2CdI_4 (at 417(2) K) $\rightarrow$ β-AgI + CdI_2 + β-Ag_2CdI_4 + ε-Ag_2CdI_4 (at 366(2) K). These are in agreement with the x-ray diffraction results and the reported phase diagram for the AgI–CdI_2 system [9].

3.3. Neutron diffraction results: Ag_2ZnI_4

In agreement with earlier studies [10, 13], the observed neutron diffraction pattern collected from the ambient temperature phase of Ag_2ZnI_4 (here labelled β-Ag_2ZnI_4) contains a series of strong reflections which can be indexed using a hexagonal unit cell with $a \sim 4.20$ Å and $c \sim 7.25$ Å, together with a large number of weak reflections. The majority of the latter are consistent with those reported previously, though significant differences are observed for the peaks at d-spacings greater than ~4.5 Å. All the peaks observed in this work were successfully indexed to give an orthorhombic unit cell with $a \approx 8.800$ Å, $b \approx 7.622$ Å and $c \approx 7.236$ Å, these having a relationship to the wurtzite (wz) unit cell of $a \approx 2a_{wz}$, $b \approx 2a_{wz} \sin 60°$

and $c \approx c_{wz}$. Further, since $2c/a = 1.644$ is close to the value $\sqrt{8/3} = 1.633$, the pseudohexagonal cell approximates to closest packing. The observed reflections indicate three systematic absences: $h = 2n$ for $h00$ types; $l = 2n$ for $00l$ types and $h + l = 2n$ for $h0l$ types. These are consistent with space groups $Pmn2_1$ and $Pmnm$ (a non-standard setting of $Pmmn$). However, closer inspection of the diffraction pattern indicated a possible peak at the expected position of the 201 reflection ($d \approx 3.760$ Å), though of only marginal statistical significance. If present, this would violate the last of the three conditions listed above and the resultant space group $P2_122_1$ (a non-standard setting of $P2_12_12$) was, therefore, also considered as a possible candidate for β-Ag_2ZnI_4. As remarked above, the strong reflections can be indexed on the basis of a hexagonal unit cell of similar dimensions to that of wurtzite structured β-AgI. It is, therefore, reasonable to assume that the structure of β-Ag_2ZnI_4 also possesses an hcp I^- sublattice. The unit cell volume requires that $8 \times I^-$ be placed in the unit cell. It is possible to construct an hcp array within all three of the candidate space groups. For example, in $Pmn2_1$, two sets of $2(a)$ $0, y, z$ sites are required, with $y = 1/3$ and $z = 0$ and with $y = 2/3$ and $z = 1/2$, together with a single set of general $4(b)$ x, y, z positions with $x = 1/4$, $y = 5/6$ and $z = 0$.

Within these hcp anion arrays we assume that the Zn^{2+} are located in sites which are tetrahedrally co-ordinated to four I^-, as is the case in the binary compound ZnI_2 [21]. The same environment is also the most likely for Ag^+ (as in both wurtzite structured β-AgI [2] and zincblende structured γ-AgI [1]), though in a small number of ternary compounds, such as $AgTl_2I_3$ [22], Ag^+ is found in octahedral environments. The orthorhombic unit cell found for β-Ag_2ZnI_4 contains 16 tetrahedral and eight octahedral interstices, which must accommodate $4 \times Ag^+$ and $2 \times Zn^{2+}$. The pair of Zn^{2+} ions can only be accommodated in space groups $Pmnm$ and $P2_122_1$ in tetrahedral or octahedral sites of higher multiplicity. The possibility of fractional occupancy seems unlikely, in view of the low ionic conductivity of β-Ag_2ZnI_4 (figure 1). By contrast, the tetrahedral sites in space group $Pmn2_1$ comprise $2 \times 4(b)$ plus $4 \times 2(a)$ sites. The $4(b)$ tetrahedral sites are x, y, z positions with $x = 1/4$, $y = 1/6$ and $z = 1/8$ and with $x = 1/4$, $y = 5/6$ and $z = 3/8$. Arbitrarily, we place the $4 \times Ag^+$ in the first of these. The remaining tetrahedra formed by $2(a)$ $0, y, z$ sites have $y = 2/3$, $z = 1/8$; $1/3, 5/8$; $1/3, 3/8$ and $2/3, 7/8$. Taken together with the $4(b)$ sites occupied by Ag^+, the first two pairs of $2(a)$ sites represent the positions occupied in wurtzite β-AgI and we therefore place the Zn^{2+} in one of these (arbitrarily, the former). Simulations of the diffraction pattern with the idealized positional parameters gave a very good agreement with the measured one ($R_W \sim 3\%$). Simulations using other arrangements of the $4 \times Ag^+$ and $2 \times Zn^{2+}$ over the available tetrahedral sites produced poorer agreements and, in many cases, contained anomalously short cation–cation distances along the c-axis due to the simultaneous occupancy of pairs of tetrahedra which share a common face. Similarly, attempts to place some or all of the Ag^+ in the octahedral positions did not give a satisfactory agreement.

Least squares refinements of the diffraction data using the structural model described above were performed, with the z co-ordinate of the I3 ion fixed at a value of zero to define the otherwise arbitrary origin along the c-axis. The refinement proceeded routinely, though some oscillations in the value of R_W were observed when simultaneously varying the peak width parameters and the lattice parameters, due primarily to the strongly pseudo-hexagonal nature of the structure which causes extensive peak overlap. In turn, this led to increased uncertainties in the positional parameters. The fitted parameters are listed in table 1 and the quality of the fit is illustrated in figure 4.

Complete reaction of AgI and ZnI_2 to form β-Ag_2ZnI_4 and the accompanying ordering of the Ag^+ and Zn^{2+} over the two sites listed in table 1 appears to be rather sluggish, requiring prolonged (several weeks) annealing at temperatures slightly below the upper limit of its stability range (~480 K, see below). For example, a sample annealed at only 400(3) K for

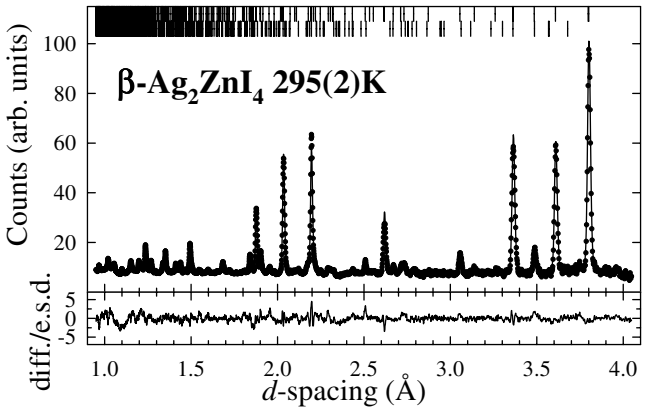

Figure 4. The least-squares fit to the powder neutron diffraction data collected from β-Ag_2ZnI_4 at 295(2) K. The dots are the experimental data points (with fitted background subtracted) and the solid curve is the calculated profile using the parameters listed in table 1. The lower trace shows the difference (measured minus calculated) divided by the estimated standard deviation on the experimental data points. The upper row of tick marks along the top of the figure denotes the calculated positions of all the symmetry allowed Bragg reflections for space group $Pmn2_1$. The lower row of ticks denotes the positions of weak additional reflections arising from a small quantity of unreacted ZnI_2 in the sample.

three weeks showed the presence of a small amount of unreacted AgI. This sample was the one used for the ionic conductivity measurements presented in figure 1 and explains the presence of the small kink at ∼420 K due to the $\beta \rightarrow \alpha$ transition in AgI. Its unit cell parameters ($a = 8.818(3)$ Å, $b = 7.618(2)$ Å and $c = 7.242(4)$ Å) are in agreement with those obtained for the sample of β-Ag_2ZnI_4 used for structural determination. However, reflection conditions indicate a space group $Pnma$ rather than $Pmn2_1$, indicating incomplete order of the Ag^+ and Zn^{2+} due to the lower sintering temperature.

As illustrated in figure 5, the diffraction pattern characteristic of β-Ag_2ZnI_4 disappears at 478(4) K and the resultant one can be attributed to a two-phase mixture of α-AgI and ZnI_2. This is essentially the behaviour published previously [15], though the earlier work reported AgI to be present in its β modification. At 538(4) K the diffraction pattern changes again, before the complete disappearance of all peaks at 598(4) K indicates melting. The diffraction pattern of α-Ag_2ZnI_4 is remarkably similar to that of β-Ag_2ZnI_4, though there is no evidence of the weaker peaks observed at ambient temperature. It is then reasonable to expect that the high-temperature phase also contains an hcp I^- sublattice, though without long-range order of the Ag^+ and Zn^{2+}. This is supported by the fact that all the observed d-spacings for α-Ag_2ZnI_4 at a temperature of 553(3) K can be successfully accounted for using a hexagonal unit cell of dimensions $a \approx 4.46$ Å and $c \approx 7.27$ Å. Comparison with the unit cell volume of the β-Ag_2ZnI_4 phase indicates that this unit cell contains only half a formula unit, i.e. $1 \times Ag^+$, $1/2\times$ Zn^{2+} and $2 \times I^-$. Furthermore, the relatively high value of ionic conductivity for α-Ag_2ZnI_4 (figure 1) indicates significant dynamic disorder of the cations, and it is likely that they occupy sites with a fractional occupancy. The observed reflections indicate that conditions $00l$ with l even and hhl with l even are required and these are consistent with space groups $P6_3mc$, $P\bar{6}2c$ and $P6_3/mmc$. However, we will restrict our discussion to tetrahedral and octahedral sites formed by the hcp iodine sublattice, in which case the space group $P\bar{6}2c$ is equivalent to $P6_3/mmc$ and we need not consider the former. To determine the correct structural description of α-Ag_2ZnI_4 we place the anions in an arrangement close to hcp and

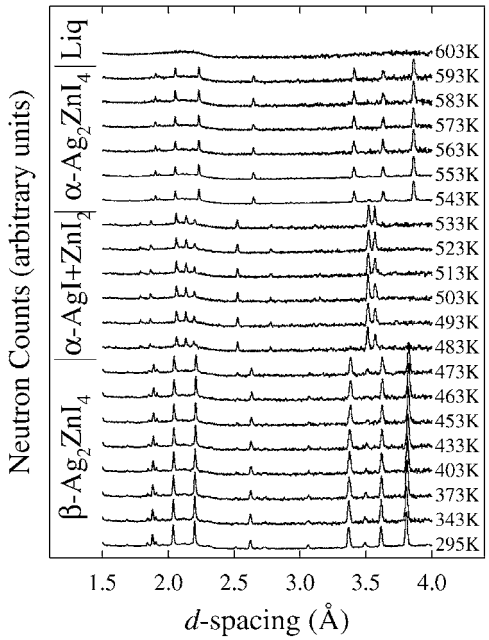

Figure 5. The evolution of a portion of the powder neutron diffraction pattern collected on heating, showing the transitions β-$Ag_2ZnI_4 \rightarrow \alpha$-AgI + ZnI_2 and α-AgI + $ZnI_2 \rightarrow \alpha$-Ag_2ZnI_4 at temperatures in the region of 478 and 538 K, respectively, followed by melting at ∼598 K.

consider different models for the cation distribution over the various tetrahedral and octahedral voids formed by the hcp anion array, assuming complete disorder of the Ag^+ and Zn^{2+} species. In space group $P6_3mc$ the I^- are then placed in the 2(b) sites at 1/3, 2/3, z and 2/3, 1/3, $z + 1/2$, with $z = 0$ and the cations are distributed over the tetrahedral sites in 2(b) positions with $z = 3/8$ such that the average occupancy is 3/4. To distribute the cations over all the tetrahedral holes it is necessary to adopt space group $P6_3/mmc$, in which the hcp anion array is formed by placing the I^- in 2(c) sites at 1/3, 2/3, 1/4 and 2/3, 1/3, 3/4. The tetrahedral interstices are then in 4(f) sites at 1/3, 2/3, z, etc with $z = 5/8$ and the octahedral voids are at 2(a) 0, 0, 0 and 0, 0, 1/2 positions. Neither of the models constraining the cations to reside in a single site provides a satisfactory fit to the diffraction data. However, a good fit with $R_W = 1.43\%$ was obtained by distributing the cations over the octahedral and tetrahedral sites in space group $P6_3/mmc$. The final fitted parameters are listed in table 1 and the quality of the fit is illustrated in figure 6.

3.4. Neutron diffraction results: Ag_3SnI_5

The initial mixture of 3AgI + SnI_2 was heated to 523(3) K on the diffractometer and left to equilibrate for ∼30 min. After this time, a short data collection indicated that the complete reaction had taken place, with no evidence of diffraction peaks due to either starting material. Diffraction data collected on cooling from 573(3) K are illustrated in figure 7, with a relatively simple diffraction pattern observed for $T > 358(4)$ K. At lower temperatures, the diffraction pattern could be indexed on the basis of SnI_2 and γ-AgI, plus additional weak peaks which are presumably due to the presence of $AgSn_2I_5$ and/or $AgSn_4I_9$ [16, 17].

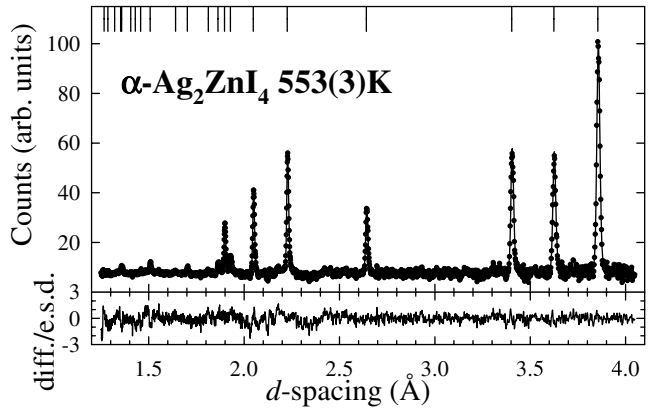

Figure 6. The least-squares fit to the powder neutron diffraction data collected from α-Ag_2ZnI_4 at 553(3) K. The dots are the experimental data points (with fitted background subtracted) and the solid curve is the calculated profile using the parameters listed in table 1. The lower trace shows the difference (measured minus calculated) divided by the estimated standard deviation on the experimental data points. The row of tick marks along the top of the figure denotes the calculated positions of all the symmetry allowed Bragg reflections for space group $P6_3/mmc$.

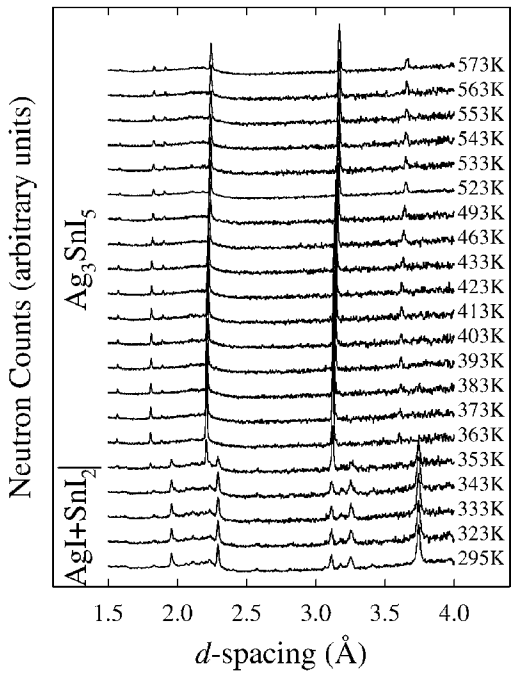

Figure 7. The evolution of a portion of the powder neutron diffraction pattern collected on cooling, showing the dissociation of Ag_3SnI_5 at a temperature of ∼358 K.

To determine the structure of Ag_3SnI_5 within its stability region we consider the data collected at 523(3) K. The d-spacings of all the observed diffraction peaks can be accounted for using a ccp unit cell with $a = 6.332$ Å, in agreement with the previous study [17]. The ionic conductivity data (figure 1) indicate that Ag_3SnI_5 is a superionic phase and we therefore

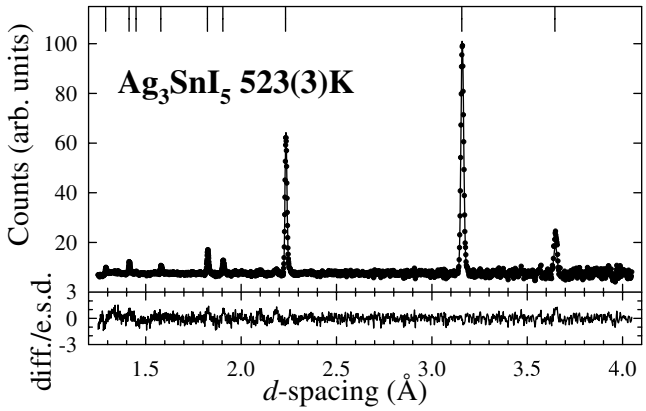

Figure 8. The least-squares fit to the powder neutron diffraction data collected from Ag_3SnI_5 at 523(3) K. The dots are the experimental data points (with fitted background subtracted) and the solid curve is the calculated profile using the parameters listed in table 1. The lower trace shows the difference (measured minus calculated) divided by the estimated standard deviation on the experimental data points. The row of tick marks along the top of the figure denotes the calculated positions of all the symmetry allowed Bragg reflections for space group $Fm\bar{3}m$.

assume that the anions form a ccp sublattice and that the two cation species are distributed randomly over the octahedral and tetrahedral interstices formed by this array. The reliability of this assumption, and the neglect of any ordering of the Ag^+ and Sn^{2+}, will be verified later by the quality of the fit to the experimental data. The size of the unit cell indicates that $4 \times I^-$ are required, which we place in the $4(a)$ 0, 0, 0 sites of space group $Fm\bar{3}m$. The unit cell contains eight tetrahedral sites in $8(c)$ 1/4, 1/4, 1/4 positions, plus four octahedral sites located in $4(b)$ 1/2, 1/2, 1/2 positions. The composition requires that we place $12/5 \times Ag^+$ and $4/5 \times Sn^{2+}$ within the ccp unit cell. Various attempts to fit the diffraction data were made, with the cations randomly distributed over the tetrahedral and/or octahedral sites of space group $Fm\bar{3}m$. In addition, refinements were performed with the cations constrained to only occupy half the tetrahedral sites using space group $F\bar{4}3m$ (i.e. only those tetrahedral positions occupied by cations in zincblende structured γ-AgI [1]). The best fit to the diffraction data ($R_W = 1.61\%$) was obtained by distributing all the Ag^+ and Sn^{2+} over the octahedral and tetrahedral interstices in space group $Fm\bar{3}m$ in the approximate ratio 4:1. The quality of the final fit to the diffraction data is illustrated in figure 8 and the final fitted parameters are listed in table 1.

4. Discussion

As illustrated in figure 9, the crystal structure of ε-Ag_2CdI_4 is closely related to that of β-Ag_2HgI_4. Both comprise a slightly distorted ccp anion sublattice, with the Ag^+, Cd^{2+} and Hg^{2+} all situated within tetrahedral cavities. As a result, both can be considered as a pair of zincblende unit cells (of the type found in γ-AgI) along the [001] direction and can be derived from the chalcopyrite structure, $CuFeS_2$ (i.e. $Cu_2Fe_2S_4$), by distributing the $4 \times Ag^+$, $2 \times M^{2+}$ in different ways over the eight tetrahedrally co-ordinated cation sites. The vacant cation sites in ε-Ag_2CdI_4 are occupied by Ag^+ in β-Ag_2HgI_4, and vice versa. By contrast, the structure of the ambient-temperature phase β-Ag_2ZnI_4 comprises an almost ideal hcp array of I^-, with the $4 \times Ag^+$ and $2 \times Zn^{2+}$ per unit cell distributed in an ordered manner over the 16 tetrahedral interstices. As such, it can be derived from the wurtzite structure (β-AgI [2]) and is a hexagonal analogue of the defect chalcopyrite structures adopted by β-Ag_2HgI_4 and ε-Ag_2CdI_4. Whilst

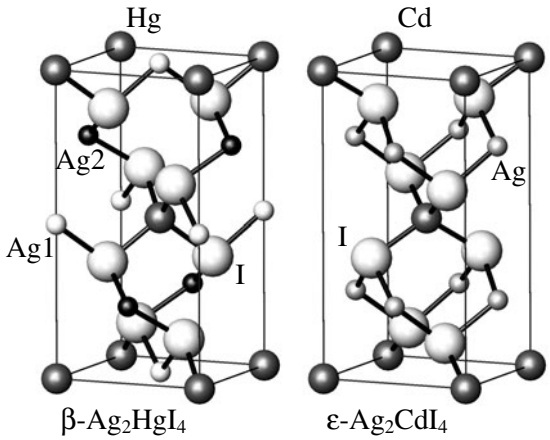

Figure 9. Comparison of the crystal structures of β-Ag_2HgI_4 (left) and ε-Ag_2CdI_4 (right). With decreasing size, the spheres denote I^-, Hg^{2+}/Cd^{2+} and Ag^+, with the different colours of the latter showing the two symmetry independent sites in β-Ag_2HgI_4.

there are examples of hcp counterparts to the ccp chalcopyrite structure (such as $LiGaO_2$ [23] and Fe_2CuS_3 [24]), β-Ag_2ZnI_4 is, to the best of the authors' knowledge, the first example of a cation deficient phase of this stoichiometry. The relationship between the crystal structures of β-Ag_2ZnI_4, $LiGaO_2$ and β-AgI is illustrated in figure 10.

The close relationship between the crystal structures of ε-Ag_2CdI_4 and β-Ag_2ZnI_4 is further demonstrated by the anion co-ordination polyhedra which surround the cation species. In the former material the four Ag–I distances are all equal at 2.798(2) Å and the six I–Ag–I angles are 106.7(1)° (× 2) and 110.88(6)° (× 4), forming a nearly regular tetrahedron. The four Cd–I distances are 2.821(3) Å and the I–Cd–I angles (106.43(6)° (×4) and 115.7(1)° (×2)) deviate further from the ideal tetrahedral value of $2\sin^{-1}\sqrt{2/3} = 109.47°$. Tetrahedral co-ordination of Cd^{2+} to I^- is relatively common, though the binary phase CdI_2 is widely known to adopt numerous polytypes based on different packings of edge sharing, nearly regular, CdI_6 octahedra (see, for example [25]). In the case of β-Ag_2ZnI_4, the Ag^+ tetrahedra possess Ag–I distances of 2.688(8), 2.701(8), 2.721(9) and 2.753(8) Å and six different I–Ag–I angles in the range 108.0°–110.4°, whilst the Zn^{2+} centred tetrahedra are more distorted, with Zn–I distances of 2.627(7) Å (×2), 2.785(11) and 2.789(11) Å and I–Zn–I angles ranging from 106.1° to 116.3°. This mirrors the situation in the binary halides, where the cation centred tetrahedra found in ZnI_2 [21] are somewhat more distorted than those present in both the β and γ forms of AgI [1, 2].

As discussed in section 3.3, the unit cell dimensions of the orthorhombic β phase of Ag_2ZnI_4 can be described as a pseudo-hexagonal cell with $a_{hex} = a_\beta/2$, $a'_{hex} = b_\beta/2\sin 60°$, $c_{hex} = c_\beta$ and $c_{hex}/a_{hex} \approx \sqrt{8/3} = 1.633$. The temperature variation of a_{hex}, a'_{hex} and c'_{hex} is illustrated in figure 11. In the case of β-Ag_2ZnI_4, c_{hex}/a_{hex} has a value in the range 1.644–1.640 which is slightly larger than that characteristic of hexagonal closest packing, whilst in the α-phase the value is approximately 1.629. Within the α-Ag_2ZnI_4 phase, the disordered Ag^+ and Zn^{2+} predominantly occupy the tetrahedral interstices, with a significant fraction residing in the octahedral sites. This suggests that cation diffusion occurs predominantly between tetrahedral cavities via the octahedral ones. A similar situation is observed in the high-temperature superionic phase δ-Ag_2HgI_4 [7].

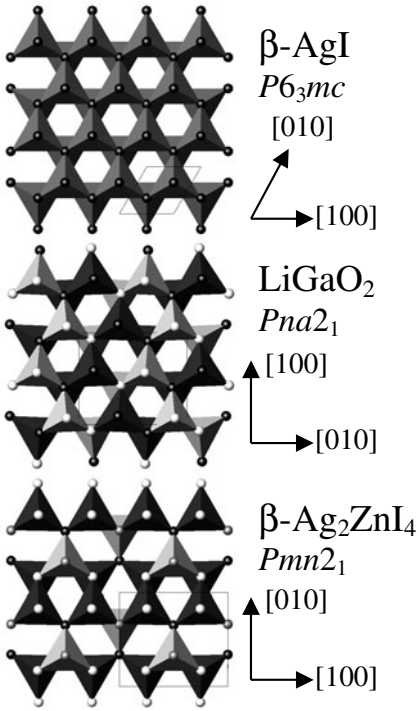

Figure 10. Comparison of the crystal structures of β-AgI (top) [1], $LiGaO_2$ (middle) [26] and β-Ag_2ZnI_4 (bottom), highlighting the similarities between the packing of their tetrahedra. The darker and lighter tetrahedra denote Ag^+/Li^+ and Ga^{3+}/Zn^{2+} centred units, respectively.

The high-temperature superionic phase adopted by Ag_3SnI_5 can be considered as a ccp counterpart to the hcp based structure of α-Ag_2ZnI_4. There are two other superionic AgI–MI_2 phases which adopt ccp anion sublattices, Ag_4PbI_6 [8] and α-Ag_2HgI_4 [6]. The time-averaged structure of Ag_3SnI_5 is more similar to the former, since the $Ag^+ + M^{2+}$ species reside predominantly within the octahedral interstices, rather than half of the tetrahedral ones (as in the case of α-Ag_2HgI_4 [6]). In the binary compound SnI_2 [26], there are two symmetry independent Sn^{2+} ions, both of which are surrounded by a rather irregular octahedron of anions. The structural behaviour of Ag_3SnI_5 on increasing temperature is illustrated in figure 12. Of particular significance is the temperature dependence of the cation site occupancies, which show a steady increase in the population residing on tetrahedral interstices. Whilst m_{tet} increases by a factor of around two over the temperature range studied, there is only a modest increase in the ionic conductivity σ (figure 1). This implies that, in this particular phase, the diffusion mechanism is relatively insensitive to the details of the $Ag^+ + Sn^{2+}$ distribution over the available sites. Similar observations have been made in the case of Ag_4PbI_6 [8].

Of all the Ag^+-rich phases studied here, Ag_2HgI_4 is particularly interesting since it is, to the authors' knowledge, the only compound to undergo temperature induced transitions between superionic phases formed by ccp (α), hcp (δ) and bcc (ε) anion arrays. As such, the behaviour of the ionic conductivity (figure 1) provides a direct insight into the influence of the immobile sublattice on the ionic diffusion process. The Ag^+ and Hg^{2+} cations are completely disordered and predominantly occupy tetrahedral sites in all three phases [6, 7]. On these grounds, the significantly higher value of σ within the bcc structured ε-Ag_2HgI_4 can be attributed to the

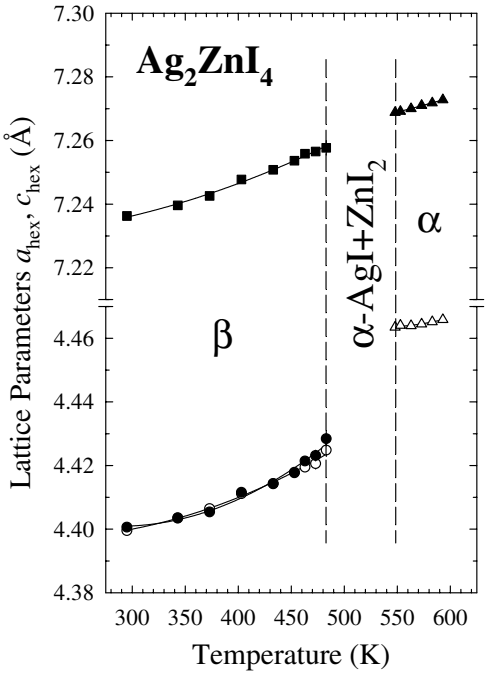

Figure 11. Temperature dependence of the hexagonal lattice parameters a_{hex} (open triangles) and c_{hex} (filled triangles) of α-Ag_2ZnI_4 and of the pseudo-hexagonal lattice parameters $a_{hex} = a_\beta$ (open circles), $a'_{hex} = b_\beta/2 \sin 60°$ (filled circles) and $c_{hex} = c_\beta$ (filled squares) of β-Ag_2ZnI_4.

greater number of available sites in this case (six per anion) than in ccp and hcp (both have two per anion) [27]. Such simple geometric arguments may also account for the slight decrease in σ at the $\alpha \rightarrow \delta$ transition, since the anion tetrahedra share only edges in the former (ccp) phase but also have some common faces in the latter (hcp) one. Although face-sharing tetrahedra might be expected to provide an easy conduction pathway, the close proximity of these pairs of face sharing tetrahedral sites does not allow both to be occupied simultaneously, effectively halving the number of available sites within the hcp sublattice and reducing σ accordingly.

We conclude the discussion with a brief overview of the structure–property relationships within Ag^+-rich phases of AgI–MI_2 systems. As illustrated in figure 13, for the $M = Cd^{2+}$ and Zn^{2+} cases increasing temperature produces dissociation and the abrupt increases to relatively high values of ionic conductivity result from the formation of free AgI. However, the addition of Hg^{2+}, Pb^{2+} and Sn^{2+} produces a reduction in the superionic transition temperature compared to pure AgI, though this effect is only slight in the latter two cases. In those cases where bcc structured superionic phases are observed (ε-Ag_2HgI_4 and α-Ag_2CdI_4) their stability range is shifted to much higher temperatures than α-AgI. Instead, the lowest superionic phases observed on heating in Ag_2HgI_4, Ag_3SnI_5 and Ag_4PbI_6 are based on a ccp sublattice. As discussed previously [8], the addition of M^{2+} cations may destabilize the bcc sublattice relative to the ccp one because the latter provides more favourable environments for the divalent species, whether this is predominantly tetrahedral ($M = Hg^{2+}$) or octahedral ($M = Sn^{2+}$ and Pb^{2+}). This is a direct consequence of the specific geometries of the two sublattices, because the tetrahedral and octahedral interstices with the bcc sublattice are both distorted (the tetrahedral interstices have I–cation–I angles of $2 \sin^{-1} \sqrt{3/5} = 101.54°$ and $2 \sin^{-1} \sqrt{4/5} = 126.87°$,

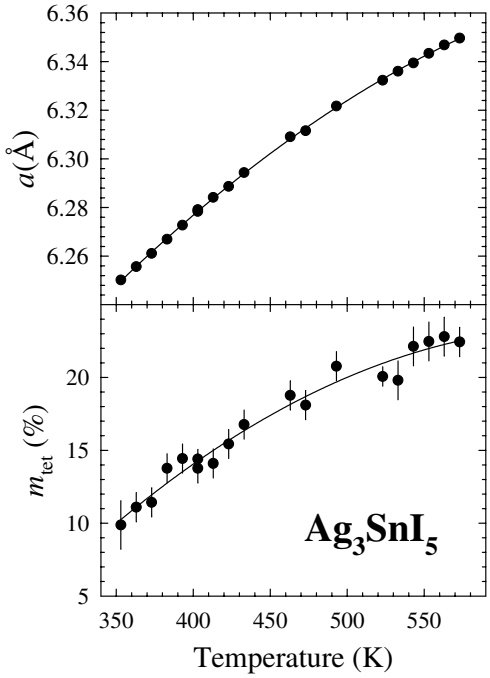

Figure 12. Temperature dependence of the cubic lattice parameter a (top) and the mean fraction of cations residing on the tetrahedral sites m_{tet} (bottom) of Ag_3SnI_5.

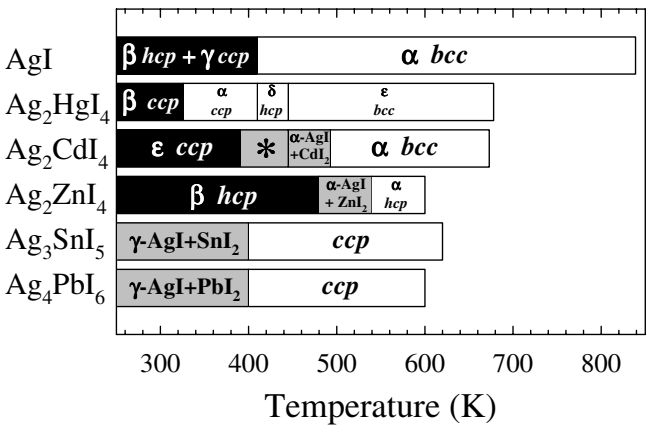

Figure 13. Schematic diagram summarising the structural behaviour of Ag-rich phases in AgI–MI_2 systems (data from this work and from [5–10]). Black shading indicates low conductivity phases, grey denotes mixed phase regions, whilst superionic phases have a white background. In the case of Ag_2CdI_4, the region labelled $*$ is a mixture of β-Ag_2CdI_4, β-AgI and CdI_2.

rather than the ideal value of $2\sin^{-1}\sqrt{2/3} = 109.47°$ and the octahedral holes have four cation–I distances of $a/\sqrt{2}$ plus two shorter contacts of $a/2$), whereas both are regular in ccp. The marked reduction in the ionic conductivity of the ccp phases (compared to bcc α-AgI) can, of course, be attributed to the number of sites available for the diffusing cations, since the

argument presented in the previous paragraph concerning the tetrahedral sites also holds for the octahedral interstices (one per anion in ccp and three per anion in bcc).

5. Conclusions

The results presented in this paper highlight the ability of the Ag^+ to undergo rapid diffusion within different anion sublattices. Whilst the cost disadvantages of silver remain a barrier to any commercial exploitation, the systematic study of the ionic arrangements and ionic conductivities of phases in the AgI–MI_2 systems provides a direct insight into the fundamental structure–property relationships within this important family of superionic conductors. The Ag^+-rich phases in all five cases ($M = Cd^{2+}$, Hg^{2+}, Pb^{2+}, Sn^{2+} and Zn^{2+}) either only exist in high-temperature superionic phases (Ag_3SnI_5 and Ag_4PbI_6) or adopt high-temperature modifications which have exceptionally high ionic conductivities (Ag_2CdI_4, Ag_2HgI_4 and Ag_2ZnI_4). This behaviour mirrors the situation in the AgI–M′I in which all phases of stoichiometry AgM'_2I_3, $AgM'I_2$ and $Ag_2M'I_3$ possess ionic conductivities less than $\sim 10^{-5}\ \Omega^{-1}\ cm^{-1}$ [28] whilst both known compounds of composition $Ag_4M'I_5$ (Ag_4RbI_5 and Ag_4KI_5) have amongst the highest values of σ at ambient temperature [29–31].

Acknowledgments

The work presented in this paper forms part of a wider project investigating the structural properties of superionic conductors funded by the Engineering and Physical Sciences Research Council (reference GR/M38711). One of the authors (PB) wishes to thank the Swedish Research Council for financial support.

References

[1] Burley G 1963 *J. Chem. Phys.* **38** 2807
[2] Adams L H and Davis B L 1962 *Proc. Natl Acad. Sci. USA* **48** 983
[3] Nield V M and Hayes W 1995 *Defect Diffusion Forum* **125/126** 37
[4] Wright A F and Fender B E F 1977 *J. Phys. C: Solid State Phys.* **10** 2261
[5] Nield V M, Keen D A, Hayes W and McGreevy R L 1993 *Solid State Ion.* **66** 247
[6] Hull S and Keen D A 2000 *J. Phys.: Condens. Matter* **12** 3751
[7] Hull S and Keen D A 2001 *J. Phys.: Condens. Matter* **13** 5597
[8] Hull S, Keen D A and Berastegui P 2002 *Solid State Ion.* **147** 97
[9] Brightwell J W, Buckley C N, Miller L S and Ray B 1983 *Phys. Status Solidi* a **76** 391
[10] Brightwell J W, Buckley C N, Hollyoak R C and Ray B 1984 *J. Mater. Sci. Lett.* **3** 443
[11] Natarajan M and Secco E A 1981 *Can. J. Chem.* **59** 2685
[12] Bolesta A M and Futei A V 1991 *Neorg. Mater.* **27** 2406
[13] Fourcroy P H, Rivet J and Flahaut J 1974 *C. R. Acad. Sci., Paris* C **278** 1189
[14] Ammlung R L, Scaringe R P, Ibers J A, Shriver B F and Whitmore B H 1979 *J. Solid State Chem.* **29** 401
[15] Blachnik R and Stöter U 1989 *Thermochim. Acta* **145** 93
[16] Blachnik R and Stöter U 1987 *Thermochim. Acta* **112** 47
[17] Wojokowska A, Kundys E and Josiak J 1996 *J. Mater. Sci.* **31** 2425
[18] Hull S, Smith R I, David W I F, Hannon A C, Mayers J and Cywinski R 1992 *Physica* B **180/181** 1000
[19] Larson A C and Von Dreele R B 1994 *Los Alamos National Laboratory Report* LAUR 86-748
[20] Gardner N J G, Hull S, Keen D A and Berastegui P 1998 *Rutherford Appleton Laboratory Report* RAL-TR-1998-032
[21] Fourcroy P H, Carré D and Rivet J 1978 *Acta Crystallogr.* B **34** 3160
[22] Hoyer M and Hartl H 1996 *Z. Anorg. Allg. Chem.* **622** 308
[23] Marezio M 1965 *Acta Crystallogr.* **18** 481

[24] Szymanski J T 1974 *Z. Kristallogr.* **140** 218
[25] Verma A M and Krishna P 1966 *Polymorphism and Polytypism in Crystals* (New York: Wiley)
[26] Howie R A, Moser W and Trevena I C 1972 *Acta Crystallogr.* B **28** 2965
[27] Boyce J B and Huberman B A 1979 *Phys. Rep.* **51** 189
[28] Yamamoto O 1993 *Fast-Ion Transport in Solids (NATO ASI Series E)* vol 250, ed B Scrosati, A Magistris, C M Mori and G Mariotto (Dordrecht: Kluwer) p 203
[29] Bradley J N and Greene P D 1966 *Trans. Faraday Soc.* **62** 2069
[30] Bradley J N and Greene P D 1967 *Trans. Faraday Soc.* **63** 424
[31] Hull S, Keen D A, Sivia D S and Berastegui P 2002 *J. Solid State Chem.* **165** 363